PIER C

(Received 29 August 2025, Accepted 15 October 2025, Scheduled 18 November 2025)

Wearable Multistatic Antenna Configuration on a Denim Substrate for Medical Imaging

Anju Mariai*, Thathamkulam A. Anjit, and Palayyan Mythil

Cochin University of Science and Technology, Cochin, Kerala, India

ABSTRACT: In this work, a multistatic antenna configuration with Compact Textile Wearable Antennas (CTWAs) is proposed for microwave imaging. The setup includes eight CTWA antennas printed on a denim jeans fabric wrapped around a phantom with a foam layer in between. The phantom is made of Delrin and is intended to replicate the breast tissue. It contains three PVC inclusions that mimic the tumors with sizes of 6 mm, 10 mm, and 3 mm. These inclusions are located at the center, near the outer surface, and between the center and the outer surface. The CTWA antennas surrounding the phantom collects the scattered data for further processing. Distorted Born Iterative Method (DBIM), along with the Reweighted Basis Pursuit (RWBP), a convex optimization algorithm, is used to reconstruct the object profile. RWBP is an iterative reconstruction algorithm in the sparse domain capable of extracting the size, shape, location, and dielectric distribution of the inclusions. The experiment is conducted using two different approaches. In one approach, multistatic without rotation, the receiver antenna is fixed at positions 0°, 45°, 90°, 135°, 180°, 225°, 270°, and 315°. In the other approach, multistatic with rotation, the receiver antenna is rotated in steps of 9° about the center of the phantom to achieve angles in between. In the multistatic configuration without rotation, the inclusions of 10 mm, 6 mm, and 3 mm were detected with errors of 0.125, 0.35, and 0.433, respectively, while in the case of multistatic configuration with rotation, the inclusions were detected with errors of 0.070, 0.066, and 0.03, respectively. The results obtained are compared with the previous studies available in the literature. These results demonstrate that the proposed wearable multistatic antenna configuration is suitable for medical imaging applications, enabling better target detection, localization, comfort, and flexibility.

1. INTRODUCTION

Microwave imaging (MWI) is an effective technique that uses non-ionizing radiation to visualize the human body without physical contact or causing any harm to the tissues [1]. This approach has gained attention in the medical field due to its broad range of applications and high level of safety. MWI is used for a variety of applications, such as medical imaging, nondestructive testing, industrial process monitoring, security screening, and through wall imaging [2]. The effectiveness of MWI arises from its ability to distinguish between malignant and healthy tissues based on differences in their dielectric properties [3]. Among these applications, breast cancer detection remains a particularly important focus, as early diagnosis significantly improves patient survival rates compared to detection at advanced stages [4]. Consequently, there is an increasing demand for diagnostic methods that are safe, cost-effective, nondestructive, and noninvasive. Several techniques such as ultrasound, MRI, PET, and CT scans are available for medical imaging [5]. Though these methods have their own advantages, they also present challenges such as high cost, time consumption, and concerns about potential long-term health risks. In contrast, MWI is a promising alternative that overcomes many of these challenges. It is safer, more comfortable, and noninvasive, with the potential to provide effective results at a lower cost and without the risks of ionizing radiation.

The tomographic, or quantitative, approach efficiently reconstructs the distribution of the tissue permittivity and conductivity, thereby enabling more detailed detection and characterization of the abnormalities such as tumors [6]. This approach enables the estimation of the permittivity profile of the scatterer by solving nonlinear and ill-posed Inverse Scattering Problem (ISP) using measured scattered field. A typical tomographic (quantitative) imaging system essentially consists of components such as the test object, transmitting and receiving antennas, a data acquisition system, and an image reconstruction algorithm.

Transmitting and receiving antennas are crucial in microwave imaging (MWI), as they send and receive microwave signals that interact with the object. Their design, placement, and performance directly impact the quality and accuracy of the final images. The design of antennas for microwave imaging involves several key challenges, such as minimizing physical size, integrating a larger number of antennas, and reducing the need for mechanical movement [7]. Various types of antennas, such as monopole antennas, fractal antennas, Vivaldi antennas, slot antennas, and rigid patch antennas [8–12], have been developed for microwave imaging. In addition, flexible and wearable antennas [13] have been used to provide an effective solution, offering flexibility, comfort, improved mobility, non-intrusiveness, ease of integration, and portability.

* Corresponding author: Anju Maria (anjumaria@cusat.ac.in).

In the data acquisition phase, based on the antenna locations and mode of operation, there are three types of antenna configurations: monostatic, bistatic, and multistatic ones. Monostatic systems are simple to implement, but they suffer from limited angular diversity and are more prone to motion artifacts [14]. Bistatic systems have improved target detection and reduced jamming. However, bistatic systems also have less spatial diversity and coverage [15]. Multistatic setups have enhanced target detection, localization, and tracking by utilizing the spatial diversity provided by multiple transmitter-receiver combinations. It also improves system robustness, as the failure of one node does not significantly impact overall performance [16]. Though the multistatic setup has the above-mentioned advantages, the number of transmitters/receivers that can be accommodated without mutual coupling and overlapping is limited. Hence, it is not suitable for medical imaging applications which need more accurate results for prediction. In the above-mentioned three modes, the receiving antenna can be further rotated to different positions, which can increase spatial diversity and coverage [17–20]. In [21–23], antennas operate in multistatic mode for microwave imaging. The works [21] and [22] employ rigid antennas fabricated on FR4 and GIL GML 1032 substrates, respectively, for breast tumor detection and brain injury detection. Ref. [23] utilizes a flexible Kapton substrate for breast tumor detection. Rigid substrates make it difficult for antennas to conform to curved or uneven surfaces and reduce the ease of system integration into portable or wearable imaging devices. This limits their applicability in medical imaging and on-body scanning applications. On the other hand, flexible and wearable multistatic antennas offer better adaptability and comfort in such scenarios. However, only a limited number of studies have been reported in the literature employing multistatic wearable antennas in microwave imaging.

This paper proposes a denim based compact and integrated multistatic wearable antenna configuration with eight CTWAs for microwave imaging (MWI) in medical applications. These eight CTWAs [24] use a denim jeans substrate with a relative permittivity (ϵ_r) of 1.77 and loss tangent ($\tan\delta$) $= 0.03034$. The antennas are wrapped around the phantom, and measurements are carried out in an anechoic chamber. The experiment is carried out using two different approaches. In the first approach, the receiving antenna is fixed, representing a multistatic configuration without rotation. In the second approach, the receiving antennas are rotated to acquire additional data to improve spatial diversity. The scattered fields are measured in the presence of the phantom, while the incident field is measured in its absence. From the scattered data, the object profile of the phantom is reconstructed using the RWBP algorithm. The results of the multistatic antenna configuration with and without rotation are compared with other existing results in the literature. The paper is organized as follows. Section 2 explains the microwave imaging scenario and imaging algorithm. Section 3 shows the microwave imaging experimental results, and Section 4 gives the conclusion.

2. MICROWAVE IMAGING SCENARIO AND IMAGING ALGORITHM

Quantitative Microwave imaging (MWI) employs a tomographic approach to retrieve electromagnetic properties of the scatterers (object undet test). This involves solving the nonlinear equations that relate unknown dielectric properties to the scattered fields measured by the antennas. The object under study is assumed to be inhomogeneous, characterized by the dielectric permittivity ϵ and conductivity μ. It is embedded in a homogeneous background medium with permittivity ϵ_b and conductivity μ_b. The tomographic process in MWI involves solving both the forward and inverse scattering problems.

In the tomographic arrangement, the object is illuminated by a transverse magnetic (TM) polarized wave. A set of N transmitters and M receiving antennas are positioned uniformly around the object, as shown in Fig. 1. The purpose of MWI is to determine dielectric properties of the object being studied. The scattered fields resulting from the illumination are measured by the M receiving antennas. The process of obtaining the scattered fields resulting from the transmitted input is known as the forward scattering problem. The object domain/imaging domain are as shown in Fig. 1. The total field ($E^{tot}(r)$) within the imaging domain can be related as the sum of incident field ($E^{i}(r)$) and scattered field ($E^{sc}(r)$).

$$E^{tot}(r) = E^{i}(r) + E^{sc}(r) \tag{1}$$

where r represents the distance from the origin to any point within the imaging domain. The electric field integral equation (EFIE) is used to derive the total field as given in Equation (2) and solved using Method Of Moment (MOM).

$$E^{tot}(r) = E^{i}(r) + \omega^2\mu \int_V G(r,\acute{r})\Delta\epsilon(\acute{r})E^{tot}(\acute{r})d\acute{r} \tag{2}$$

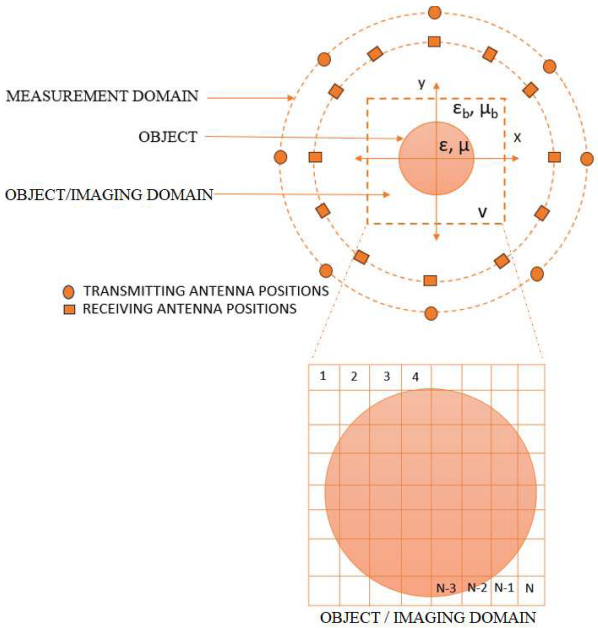

FIGURE 1. Tomographic arrangement.

$G(r, \acute{r}) - Green's\ function$
$\Delta\epsilon(\acute{r}) - Dielectric\ contrast\ function$
$\omega - Angular\ frequency$
$\mu - Permeability\ of\ the\ scatterer$
$\acute{r} - Distance\ from\ the\ origin\ to\ any\ point\ within\ the\ measurement\ domain.$

The discretized Electric Field Integral Equation (EFIE) can be expressed in the matrix form [18], as given by Equation (3).

$$[E^{sc}] = [G]\left[E^{tot}\right][\Delta\epsilon] \tag{3}$$

The dielectric profile of the object under investigation is obtained by solving Equation (3). A combination of DBIM and RWBP methods is employed for the reconstruction process. The reconstruction begins with initializing the dielectric values of the object profile. An initial estimate of the object profile is determined using the Born approximation. This approach approximates the nonlinear Inverse Scattering Problem (ISP) using an underdetermined set of linear equations. At each iteration of the DBIM algorithm, the contrast function ($\Delta\epsilon$) is estimated by solving the resulting linear equation. The algorithm alternates between solving the forward and inverse problems iteratively until it converges to a stable solution for the contrast function. The inverse problem discussed above is expressed in linear form as

$$y_{M\times 1} \approx \Phi_{M\times N}\, x_{N\times 1} \tag{4}$$

where ϕ represents measurement matrix, x the contrast function(unknown), y the measured scattered field, M the number of field values measured, and N the number of unknowns in inverse imaging. The number of unknowns N is significantly larger than the number of measurements M, making the system ill-posed. To reduce ill-posedness, compressive sensing is used, which relies on the signal's sparsity and the incoherence of the sensing matrix. The profile to be reconstructed is assumed to be complex and is represented by vector $x \in \mathbb{C}^N$. To enable a sparse representation, an orthonormal basis $\Psi \in \mathbb{C}^{N\times N}$ is chosen. Here, decomposition vector $\alpha \in \mathbb{C}^N$ is defined such that it satisfies $x \equiv \Psi\alpha$. The signal is defined as sparse when its decomposition has only K non-zero coefficients, with K being much smaller than N. The resulting ill-posed problem is given by

$$y = \Theta\alpha + n, \quad \text{where} \quad \Theta = \Phi\Psi \in \mathbb{C}^{M\times N} \tag{5}$$

Here, y is the measurement vector, α the unknown sparse signal to be recovered, and $n \in \mathbb{C}^M$ the additive noise, assumed to be independent and identically distributed. The goal is to recover α by finding the sparsest solution, subject to the constraint

$$\min_{\bar{\alpha}\in\mathbb{C}^N} \|\bar{\alpha}\|_0 \quad \text{subject to} \quad \|y - \Theta\bar{\alpha}\|_2 \le \zeta \tag{6}$$

The ℓ_0 norm, $\|\bar{\alpha}\|_0$, counts the number of non-zero elements in $\bar{\alpha}$, and ζ is the upper bound on the ℓ_2 norm of the residual noise n. Since the ℓ_0 norm is discrete and non-continuous, solving the above equation is Non-deterministic Polynomial time (NP) complete. From the possible solutions to $\Theta\alpha = y$, the one with the smallest ℓ_1 norm is chosen. However, real signals are often not perfectly sparse and may contain noise. The problem becomes recovering an approximately sparse signal x from noisy measurements. In this case, Basis Pursuit Denoising (BPDN) or Least Absolute Shrinkage and Selection Operator (LASSO) [25] minimizes the ℓ_1 norm of the coefficients, subject to a constraint on the ℓ_2 norm of residual noise n.

$$\min_{\bar{\alpha}\in\mathbb{C}^N} \|\bar{\alpha}\|_1 \quad \text{subject to} \quad \|y - \Theta\bar{\alpha}\|_2 \le \zeta \tag{7}$$

while ℓ_0 minimization focuses on reducing the magnitude of coefficients, ℓ_0 minimization targets sparsity by counting non-zero elements. Under specific conditions in compressive sensing, both approaches can lead to the same solution [26]. To approximate ℓ_0 more closely, Candès et al. proposed a reweighted ℓ_1 minimization method, which is effective when prior signal information is available [27].

Here, the Reweighted Basis Pursuit (RWBP) algorithm [18], based on compressive sensing, is used for reconstructing the object profile. The reweighted basis pursuit algorithm solves a sequence of weighted l_1 norm minimization defined as follows,

$$\min \left\|W\Psi^T\bar{x}\right\|_1 \ constrained\ by\ \|y - \Phi\bar{x}\|_2 \le \epsilon,\ \ \bar{x} \ge 0 \tag{8}$$

where W represents the matrix of positive weights, and Ψ represents the orthonormal basis function. The weights for the subsequent iteration are computed based on the current solution values, using the function $f(\gamma, x)$.

$$f(\gamma, x) \equiv \frac{\gamma}{\gamma + |x|} \tag{9}$$

where γ represents the stabilization parameter. The scaling of weight is controlled using a rate parameter β, where $0 < \beta < 1$ such that $\gamma^t \to 0$ as $t \to \infty$. The reweighted process proceeds as long as the relative difference between successive solutions remains above the threshold η, or until the maximum number of allowed iterations is reached.

3. MICROWAVE IMAGING: EXPERIMENTAL SETUP AND RESULTS

This section discusses the experimental setup for multistatic configuration with and without rotation employed for medical imaging applications.

The multistatic microwave imaging setup used to collect scattered data (Fig. 2) consists of the object under test (a phantom containing three inclusions), a transmitting antenna (Horn antenna), eight receiving antennas (CTWAs) arranged in a multistatic configuration, a network analyzer (PNAE 8362B Agi-

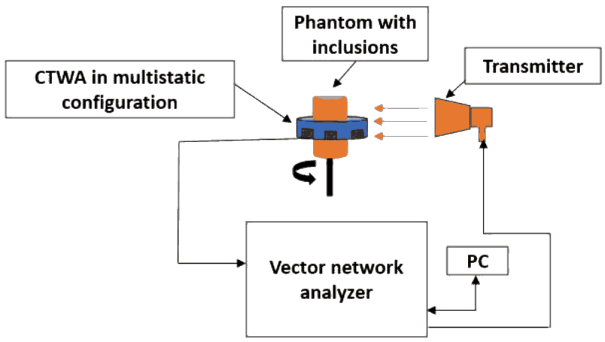

FIGURE 2. Measurement setup — Multistatic configuration.

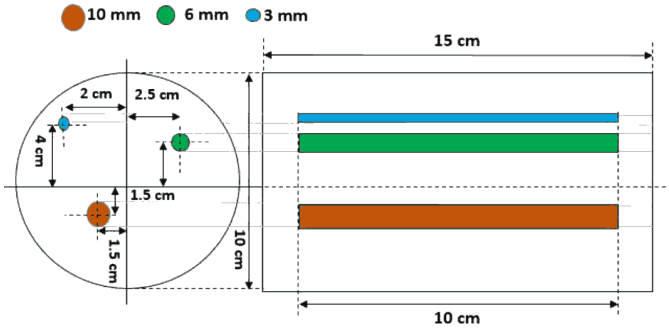

FIGURE 3. Radial and axial cross section of the phantom.

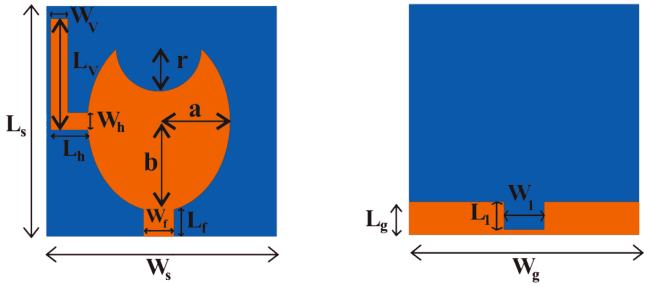

FIGURE 4. Top and bottom view of the CTWA [24].

lent), and a personal computer used to control the measurement process. Eight CTWAs are wrapped around the phantom with a foam layer in between. The scattered data are collected for both cases: multistatic configurations with and without rotation. Initially, the scattered field is measured for the multistatic configuration without rotation. After that, the antenna setup is further rotated in small increments, and additional scattered data are collected.

The object under test [17] is a dielectric cylinder with a radius of 5 cm, made of Delrin, which has a relative permittivity (ϵ_r) of 3.7. This phantom is designed to mimic breast tissue. It is made of Delrin and shaped as a solid cylinder with a total height of 15 cm. It contains three inclusions made of polyvinyl chloride (PVC) $(\epsilon_r = 4.8)$ with diameters 10 mm, 6 mm, and 3 mm. One inclusion is positioned near the periphery of the phantom, another at its center, and the third is located between the center and periphery. These inclusions represent the tumors embedded in the breast phantom. All inclusions are of length 10 cm. The radial and axial cross-sections of the phantom are shown in Fig. 3.

The transmitter horn antenna operates in the 2–18 GHz frequency range, and the receiver antenna is a Compact Ultra-Wideband (UWB) Textile Wearable Antenna (CTWA). Section 3.1 gives the details about CTWA.

3.1. CTWA

The substrate used for the CTWA [24] is denim jeans with a relative permittivity (ϵ_r) of 1.77. Denim is a flexible, durable, and comfortable material making it well suited for wearable antennas. It conforms to curved body surfaces for improved coupling and maintains its properties under bending and stretching [28]. The CTWA has a low profile, with dimensions measuring $27 \times 28 \times 0.7$ mm, and operates in the frequency range of 3.01 to 15.98 GHz. The CTWA exhibits a higher fractional bandwidth of 137%, an efficiency of 90.11%, and a gain of 5.81 dBi compared to other flexible antennas made from felt, foam, cotton, etc. [24]. A self-adhesive conductive tape is used as the radiating element, and a 50 ohm SMA connector serves as the microstrip feed line. The geometry and dimensions of the CTWA are as shown in Fig. 4 and Table 1, respectively. The antenna fabricated on the denim jeans substrate is shown in Fig. 5. The Specific Absorption Rate (SAR) obtained for the CTWA at 4, 7, and 10 GHz is 1.2, 1.08, and 1.58 W/kg, respectively, and is within the permissible limit specified by the Federal Communications Commission (FCC). The simulated and measured reflection coefficient curves of the CTWA are as shown in Fig. 6.

FIGURE 5. Fabricated prototype of the CTWA [24].

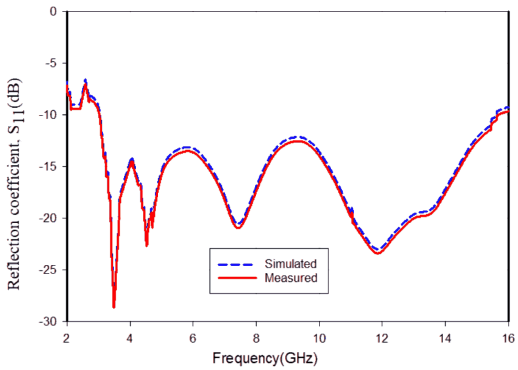

FIGURE 6. Reflection coefficient versus frequency plot of the CTWA.

3.2. Experimental Setup and Procedure

Eight CTWAs (receiving antennas) are printed on denim fabric and wrapped around the phantom with a foam layer of thickness 3 cm in between as shown in Fig. 7. The length of the denim cloth used for wrapping is 59.8 cm. The antennas are wrapped such that the radiating faces are oriented inwards facing the phantom. An inter-element spacing of approximately $\lambda/2$ needs to be maintained between adjacent elements, as it effectively minimizes the mutual coupling and ensures stable impedance and radiation characteristics. Hence, the number of CTWAs that can be accommodated on the cloth without mutual coupling is eight. The top and bottom views of the multistatic arrangement of the CTWAs are presented in Fig. 8 and Fig. 9,

FIGURE 7. Receiving antenna setup.

respectively. Since there are eight antennas, the antennas are positioned at 45-degree intervals, specifically at 0°, 45°, 90°, 135°, 180°, 225°, 270°, and 315°. The vector network analyzer is used to measure the complex transmission coefficient, S_{21}. All measurements are conducted inside an anechoic chamber, as illustrated in Fig. 10.

The object (phantom with inclusions) is positioned at the center of the turntable. For a particular illumination angle of the horn antenna (transmitting antenna), scattered data are collected at the eight receiver positions. In the first approach, the measurements are repeated for 36 views of the transmitter for 21 different frequency points between 3 and 4 GHz. The total scattered data size without rotating the receiving antenna is $36 \times 8 \times 21$. For the second approach in order to obtain additional data to achieve spatial diversity, the receiving antennas are rotated to new positions in steps of 9°. For each rotation, the scattered data are collected from the eight receiving antennas for the 36 views of the transmitter. The scattered data size for the 21 frequency points will be increased to a size of $36 \times 40 \times 21$. These data corresponding to the frequencies ranging from 3 to 4 GHz band in steps of 0.05 GHz are used to generate the final cross-sectional image of the phantom.

The DBIM combined with RWBP algorithm is employed to reconstruct the image from the data. The metric used to calculate the accuracy is the root mean square error (RMSE) [20]. It is calculated by comparing the output from the proposed method with the actual dielectric profile of the object.

$$\text{RMSE} = \sqrt{\frac{1}{M}\sum_{i}\sum_{j}\left(\frac{D^{r}_{i,j} - D^{a}_{i,j}}{D^{a}_{i,j}}\right)^{2}} \qquad (10)$$

where $D^{r}_{i,j}$ — reconstructed diameter of the inclusion produced by the proposed method, $D^{a}_{i,j}$ — actual diameter of the inclusion, M = total number of square cells in the imaging domain.

$$(i = 1, 2, \ldots, M_1; \quad j = 1, 2, \ldots, M_2; \quad M = M_1 \times M_2)$$

TABLE 1. Dimensions of the CTWA.

Sl. No	Antenna parameter	Dimensions (mm)
1	W_s (substrate-width)	28
2	L_s (length-substrate)	27
3	h (height-substrate)	0.7
4	r (semicircular slot-radius)	6.25
5	W_f (feed-width)	3
6	L_f (feed-length)	2.5
7	W_g (ground-width)	28
8	L_g (length-ground)	2
9	W_v (width-vertical strip)	2
10	L_v (length-vertical strip)	15
11	W_h (width-horizontal strip)	2
12	L_h (length-horizontal strip)	2.5
13	W_1 (width-slot)	4
14	L_1 (length-slot)	1.2

3.3. Results and Analysis

This section presents the results of the performance of the multistatic configuration employing eight CTWAs, both with and without rotation.

In the multistatic configuration (without rotation), employing eight CTWAs with a data size $8 \times 36 \times 21$, all the three inclusions measuring 10 mm, 6 mm, and 3 mm were successfully localized. The corresponding errors are 0.125, 0.35, and 0.433, respectively, as shown in Table 1. The results obtained are compared with the previous work that employed an egg-shaped rigid antenna in a bistatic mode of operation (with rotation) using the same RWBP algorithm [18]. The corresponding scattered data size in [18] was $36 \times 36 \times 21$ with errors of 0.168, 0.366, and 0.366 for the inclusions of 10 mm, 6 mm, and 3 mm. Fig. 11(a) shows the reconstructed object profile using the RWBP algorithm with a rigid egg-shaped antenna, while Fig. 11(b) shows the reconstructed profile using the RWBP algorithm with wearable CTWA antennas (proposed). It can be seen that in the proposed multistatic configuration with only eight CTWAs (without rotation) the inclusions 10 mm and 6 mm have been detected with better accuracy. Even though the data size $8 \times 36 \times 21$ is very much less than $36 \times 36 \times 21$ [18], the accuracy achieved is better/comparable. This could be attributed to the absence of errors due to rotation/movement in the proposed antenna configuration.

To further improve the performance, either the antenna size should be reduced to accommodate more antennas, or a multistatic configuration with rotation can be employed. In this work, a multistatic configuration with rotation is adopted. The receiving antennas (CTWAs) are rotated to four different positions corresponding to angles: 9°, 18°, 27°, and 36°. At each angle, measurements are taken from the eight antennas, resulting in a total of 40 measurement positions. The experiment is repeated for 36 views of the transmitter for the frequencies spanning from 3 to 4 GHz ($40 \times 36 \times 21$). Fig. 11(c) shows the reconstructed object profile of the proposed work (mul-

FIGURE 8. Multistatic arrangement: Top view.

FIGURE 9. Multistatic arrangement: Bottom view.

TABLE 2. Performance comparison of the proposed work with existing approaches.

Method/ Antenna typed	Measurement Positions	Inclusions with diameter 10 mm Location (−1.5, −1.5)			Inclusions with diameter 6 mm Location (2.5, 2.5)			Inclusions with diameter 3 mm Location (−2, 4)		
		Location	Estimated Diameter (mm)	RMSE	Location	Estimated Diameter (mm)	RMSE	Location	Estimated Diameter (mm)	RMSE
TV Norm [17]/ Rigid/ Bistatic (rotation)	36 × 36 × 21	(−1.515, −1.525)	13.4	0.340	(2.45, 2.45)	12.4	1.066	Not Detected	Nil	Nil
RWBP [18]/ Rigid/ Bistatic (rotation)	**36 × 36 × 21**	**(−1.505, −1.515)**	**8.32**	**0.168**	**(2.48, 2.50)**	**3.8**	**0.366**	**(−1.97, 4.01)**	**1.9**	**0.366**
SVBIM [19]/ Rigid/ Bistatic (rotation)	36 × 36× 21	(−1.505, −1.505)	9.11	0.089	(2.51, 2.50)	5.2	0.133	(−2, 4)	2.2	0.266
Hybrid LSQR [20]/ Rigid/ Bistatic (rotation)	36 × 36 × 21	(−1.503, −1.504)	9.15	0.085	(2.51, 2.50)	5.24	0.128	(−2, 4)	2.34	0.165
a) Proposed RWBP/ Wearable/ Multistatic (without rotation)	**8 × 36 × 21**	**(−1.505, −1.510)**	**8.75**	**0.125**	**(2.49, 2.51)**	**3.9**	**0.35**	**(−1.98, 4.01)**	**1.7**	**0.433**
a) Proposed RWBP/ Wearable/ Multistatic (with rotation)	**40 × 36 × 21**	**(−1.502, −1.503)**	**9.30**	**0.070**	**(2.50, 2.51)**	**5.6**	**0.066**	**(−2, 4)**	**2.91**	**0.03**

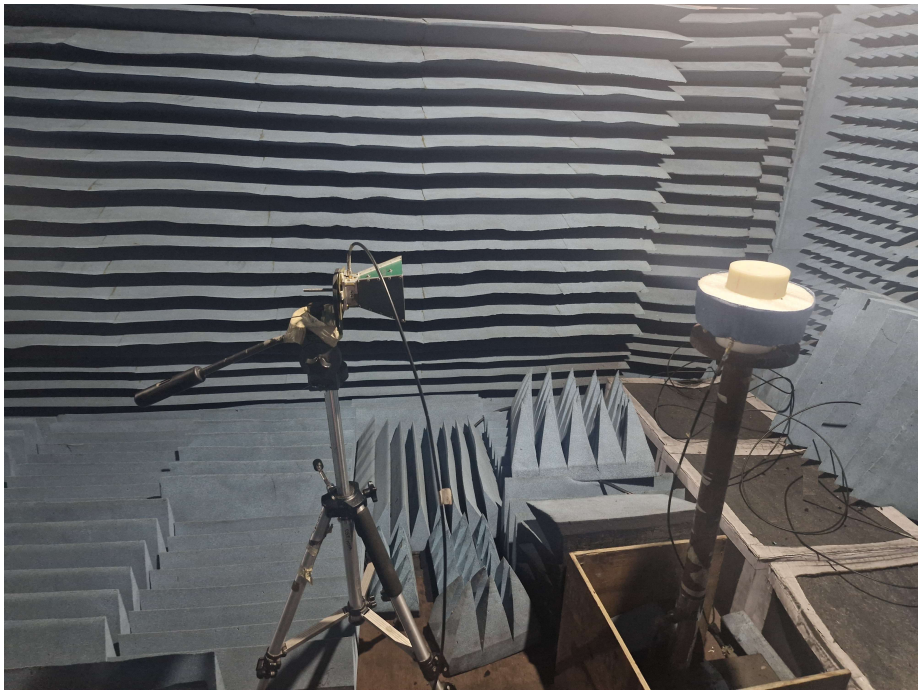

FIGURE 10. Measurement setup for multistatic configuration.

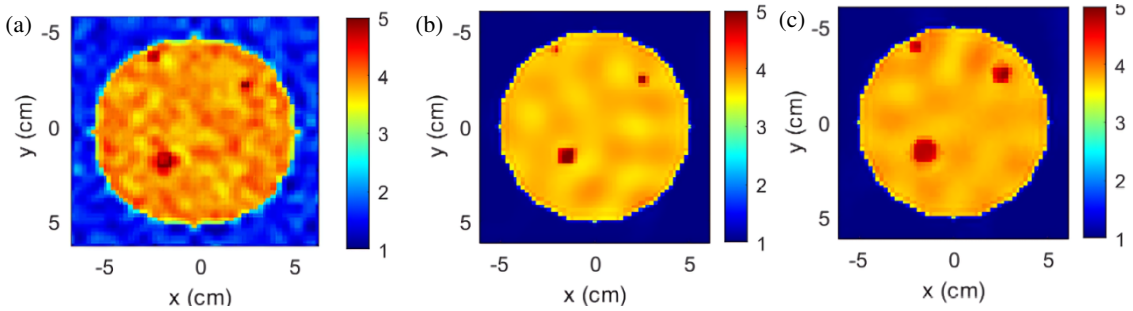

FIGURE 11. Reconstructed object profile using DBIM + RWBP — (a) rigid egg shaped antenna — bistatic configuration (with rotation) ([18]). (b) Wearable CTWA antennas-multistatic configuration without rotation (Proposed). (c) Wearable CTWA antennas — multistatic configuration with rotation (Proposed).

tistatic configuration with rotation) using wearable CTWAs. Here, all the inclusions are detected with comparitavely low error values of 0.070, 0.066, and 0.03 for the inclusions 10 mm, 6 mm, and 3 mm, respectively. Table 2 shows the performance comparison of the proposed work with [18] and other previous works reported in the literature which uses other techniques like TV (Total Variation) Norm [17], SVBIM (Subspace-based Virtual Born Iteration Method) [19] and hybrid Least Square QR (LSQR) [20] in combination with DBIM.

From the table it can be seen that the proposed method successfully detects all the inclusions with lower error than the existing works. Unlike the bistatic configuration with rigid antenna (with rotation) used in previous studies, this work improves the result by adopting a multistatic configuration with wearable CTWA. The use of wearable antennas in a multistatic arrangement provides enhanced spatial diversity, adaptability, and robustness against motion related errors, thus making the proposed multistatic configuration more suitable for medical imaging applications.

4. CONCLUSION

A multistatic wearable configuration for medical imaging using a denim jeans substrate has been proposed and experimentally validated in this paper. Compact Textile Wearable Antennas (CTWAs) are employed as the recieving antennas. The use of wearable antennas enhances the comfort and flexibility compared to rigid antennas, making them well suited for medical imaging applications. DBIM with RWBP algorithm is employed as the imaging technique for object profile detection. A study has been carried out both with and without rotating the multistatic antenna configuration. In the multistatic configuration without rotation, inclusions of 10 mm, 6 mm, and 3 mm are detected with errors of 0.125, 0.35, and 0.433, respec-

tively, whereas in a multistatic configuration with rotation, the inclusions were detected with lower errors of 0.070, 0.066, and 0.03 for 10 mm, 6 mm, and 3 mm inclusions, respectively. The proposed multistatic arrangement provides spatial diversity, robustness against motion related errors, improves detection accuracy due to the multiple observation angles, and maintains reliable performance.

REFERENCES

[1] Benny, R., T. A. Anjit, and P. Mythili, "An overview of microwave imaging for breast tumor detection," *Progress In Electromagnetics Research B*, Vol. 87, 61–91, 2020.

[2] Singh, V., S. A. Pratap, A. Kumar, P. Tripathi, and S. R. Kumar, "Microwave and millimeter-wave radar imaging: Challenges and applications," in *Microwave Devices and Circuits for Advanced Wireless Communication*, 84–98, 1st edition, D. K. Choudhary, N. Mishra, I. Singh, et al. (eds.), CRC Press, 2024.

[3] Mirbeik-Sabzevari, A., R. Ashinoff, and N. Tavassolian, "Ultra-wideband millimeter-wave dielectric characteristics of freshly excised normal and malignant human skin tissues," *IEEE Transactions on Biomedical Engineering*, Vol. 65, No. 6, 1320–1329, 2018.

[4] Bhushan, A., A. Gonsalves, and J. U. Menon, "Current state of breast cancer diagnosis, treatment, and theranostics," *Pharmaceutics*, Vol. 13, No. 5, 723, 2021.

[5] Kitson, S. L., "Modern medical imaging and radiation therapy," *Cyber Security |Big Data| AI. Open Med. Science*, 2024.

[6] Origlia, C., D. O. Rodriguez-Duarte, J. A. T. Vasquez, J.-C. Bolomey, and F. Vipiana, "Review of microwave near-field sensing and imaging devices in medical applications," *Sensors*, Vol. 24, No. 14, 4515, 2024.

[7] Lu, J., W. Wang, X. Wang, and Y. Guo, *Active Array Antennas for High Resolution Microwave Imaging Radar*, Springer, 2023.

[8] Celik, A. R. and M. B. Kurt, "Development of an ultra-wideband, stable and high-directive monopole disc antenna for radar-based microwave imaging of breast cancer," *Journal of Microwave Power and Electromagnetic Energy*, Vol. 52, No. 2, 75–93, 2018.

[9] Muqdad, Z. S., T. A. Elwi, and Z. A. A. Hassain, "A fractal antenna design for microwave radiology imaging applications," in *2021 International Conference on Computing and Communications Applications and Technologies (I3CAT)*, 23–27, Ipswich, United Kingdom, 2021.

[10] Özmen, H. and M. B. Kurt, "Radar-based microwave breast cancer detection system with a high-performanceultrawide band antipodal Vivaldi antenna," *Turkish Journal of Electrical Engineering and Computer Sciences*, Vol. 29, No. 5, 2326–2345, 2021.

[11] Liaqat, M., L. G. Costa, T. C. Vasconcelos, P. S. Lessa, E. C. Lins, L. K. B. Santos, and F. D. Nunes, "A feasible novel technique for breast cancer imaging using UWB-microwave antennas," *Journal of Clinical & Experimental Oncology*, Vol. 6, 2, 2017.

[12] Hasan, M. M., M. Samsuzzaman, M. S. Talukder, M. T. Islam, R. Azim, and M. A. Masud, "Wideband slotted patch antenna for microwave based head imaging applications," in *2020 2nd International Conference on Sustainable Technologies for Industry 4.0 (STI)*, 1–4, Dhaka, Bangladesh, 2020.

[13] Choudhary, D. K., I. Singh, M. K. Singh, and A. K. Jain, *Compact and Flexible Microwave Devices*, John Wiley & Sons, 2025.

[14] Fear, E. C., J. Bourqui, C. Curtis, D. Mew, B. Docktor, and C. Romano, "Microwave breast imaging with a monostatic radar-based system: A study of application to patients," *IEEE Transactions on Microwave Theory and Techniques*, Vol. 61, No. 5, 2119–2128, 2013.

[15] Willis, N. J. and H. D. Griffiths, *Advances in Bistatic Radar*, SciTech Publishing, 2007.

[16] Testa, A., D. Pastina, and F. Santi, "Decentralized approach for translational motion estimation with multistatic inverse synthetic aperture radar systems," *Remote Sensing*, Vol. 15, No. 18, 4372, 2023.

[17] Cherian, P., T. A. Anjit, and P. Mythili, "A compact egg-shaped UWB antenna for breast dielectric profile imaging," *International Journal of Scientific & Technology Research*, Vol. 9, No. 03, 4672–4681, 2020.

[18] Anjit, T., R. Benny, P. Cherian, and M. Palayyan, "Microwave imaging solutions for medical imaging using re-weighted basic pursuit algorithm," *Progress In Electromagnetics Research M*, Vol. 97, 13–24, 2020.

[19] Benny, R., T. A. Anjit, P. Cherian, and P. Mythili, "A combinatorial approach to quantitative microwave imaging for breast tumour profiling using SVBIM and SpaRSA," *Progress In Electromagnetics Research C*, Vol. 139, 45–57, 2024.

[20] Nharakkat, S., T. Anjit, A. Maria, and P. Mythili, "A microwave imaging solution to inverse scattering problem using distorted born iterative method with hybrid LSQR," *Progress In Electromagnetics Research B*, Vol. 112, 105–112, 2025.

[21] Asok, A. O., A. Tripathi, and S. Dey, "Breast tumors detection using multistatic microwave imaging with antipodal Vivaldi antennas utilizing DMAS and it-DMAS techniques," *International Journal of Microwave and Wireless Technologies*, Vol. 16, No. 4, 690–703, 2024.

[22] Zamani, A., A. M. Abbosh, and A. T. Mobashsher, "Fast frequency-based multistatic microwave imaging algorithm with application to brain injury detection," *IEEE Transactions on Microwave Theory and Techniques*, Vol. 64, No. 2, 653–662, 2016.

[23] Bahramiabarghouei, H., E. Porter, A. Santorelli, B. Gosselin, M. Popović, and L. A. Rusch, "Flexible 16 antenna array for microwave breast cancer detection," *IEEE Transactions on Biomedical Engineering*, Vol. 62, No. 10, 2516–2525, 2015.

[24] Maria, A. and P. Mythili, "Compact UWB wearable textile antenna for on-body WBAN applications," *Progress In Electromagnetics Research B*, Vol. 105, 43–57, 2024.

[25] Tibshirani, R., "Regression shrinkage and selection via the lasso," *Journal of the Royal Statistical Society Series B: Statistical Methodology*, Vol. 58, No. 1, 267–288, 1996.

[26] Chartrand, R. and V. Staneva, "Restricted isometry properties and nonconvex compressive sensing," *Inverse Problems*, Vol. 24, No. 3, 035020, 2008.

[27] Candès, E. J., M. B. Wakin, and S. P. Boyd, "Enhancing sparsity by reweighted ℓ_1 minimization," *Journal of Fourier analysis and applications*, Vol. 14, No. 5, 877–905, 2008.

[28] Ahamed, J., M. F. Mahmud, M. F. Ahammed, R. Mia, M. Z. Hasan, T. H. Khan, G. Q. Limon, and A. M. Shamim, "Evaluate the strength of denim goods using different washing technique," *Journal of Materials Science and Chemical Engineering*, Vol. 9, No. 03, 1, 2021.